AGU PUBLICATIONS

JGR

Journal of Geophysical Research: Oceans

RESEARCH ARTICLE

10.1002/2016JC011775

Key Points:
- Large increase in anthropogenic carbon dioxide storage in the Northeast Pacific in the last decade
- Dissolved inorganic carbon increase accompanied by deoxygenation in the oxygen minimum zone in the Northeast Pacific
- Carbonate chemistry in the Northeast Pacific is highly sensitive to anthropogenic carbon dioxide

Supporting Information:
- Supporting Information S1

Correspondence to:
Z. A. Wang,
zawang@whoi.edu

Citation:
Chu, S. N., Z. Aleck Wang, S. C. Doney, G. L. Lawson, and K. A. Hoering (2016), Changes in anthropogenic carbon storage in the Northeast Pacific in the last decade, *J. Geophys. Res. Oceans*, *121*, 4618–4632, doi:10.1002/2016JC011775.

Received 4 MAR 2016
Accepted 31 MAY 2016
Accepted article online 3 JUN 2016
Published online 2 JUL 2016

Changes in anthropogenic carbon storage in the Northeast Pacific in the last decade

Sophie N. Chu[1,2], Zhaohui Aleck Wang[2], Scott C. Doney[2], Gareth L. Lawson[3], and Katherine A. Hoering[2]

[1]Massachusetts Institute of Technology-Woods Hole Oceanographic Institution Joint Program in Oceanography/Applied Ocean Science and Engineering, Cambridge, Massachusetts, USA, [2]Department of Marine Chemistry and Geochemistry, Woods Hole Oceanographic Institution, Woods Hole, Massachusetts, USA, [3]Biology Department, Woods Hole Oceanographic Institution, Woods Hole, Massachusetts, USA

Abstract In order to understand the ocean's role as a sink for anthropogenic carbon dioxide (CO_2), it is important to quantify changes in the amount of anthropogenic CO_2 stored in the ocean interior over time. From August to September 2012, an ocean acidification cruise was conducted along a portion of the P17N transect (50°N 150°W to 33.5°N 135°W) in the Northeast Pacific. These measurements are compared with data from the previous occupation of this transect in 2001 to estimate the change in the anthropogenic CO_2 inventory in the Northeast Pacific using an extended multiple linear regression (eMLR) approach. Maximum increases in the surface waters were 11 μmol kg^{-1} over 11 years near 50°N. Here, the penetration depth of anthropogenic CO_2 only reached ~300 m depth, whereas at 33.5°N, penetration depth reached ~600 m. The average increase of the depth-integrated anthropogenic carbon inventory was 0.41 ± 0.12 mol m^{-2} yr^{-1} across the transect. Lower values down to 0.20 mol m^{-2} yr^{-1} were observed in the northern part of the transect near 50°N and increased up to 0.55 mol m^{-2} yr^{-1} toward 33.5°N. This increase in anthropogenic carbon in the upper ocean resulted in an average pH decrease of 0.002 ± 0.0003 pH units yr^{-1} and a 1.8 ± 0.4 m yr^{-1} shoaling rate of the aragonite saturation horizon. An average increase in apparent oxygen utilization of 13.4 ± 15.5 μmol kg^{-1} centered on isopycnal surface 26.6 kg m^{-3} from 2001 to 2012 was also observed.

1. Introduction

The ocean plays a significant role in regulating Earth's carbon cycle by absorbing about one-quarter to one-third of the total anthropogenic carbon dioxide (CO_2) released into the atmosphere by fossil fuel burning and land use changes [*Le Quéré et al.*, 2010; *Sabine et al.*, 2004]. Global surface ocean pCO_2 increases at a similar rate as atmospheric CO_2 at ~2 ppm yr^{-1} based on long-term time series observations at various locations in the ocean [*Bates et al.*, 2014; *Takahashi et al.*, 2009]. Yet, on local scales, physical, chemical, and biological processes can lead to variability in surface water CO_2 levels, causing disequilibrium of CO_2 between the surface ocean and the atmosphere.

As the oceanic storage capacity potentially slows down due to the increase of temperature and decrease of buffer capacity [*Levitus et al.*, 2005; *Sabine et al.*, 2004], it becomes increasingly important to characterize and quantify the ocean's ability to absorb and store anthropogenic carbon dioxide (C_{anthro}). However, making estimates of C_{anthro} is inherently difficult because it cannot be directly measured. The anthropogenic signal is relatively small compared to the large natural background and variability of the marine inorganic carbon system. In the 1990s, the World Ocean Circulation Experiment Hydrographic Program (WOCE/WHP) and Joint Global Ocean Flux Study (JGOFS) began conducting extensive surveys with high quality, seawater carbonate system measurements. Subsequently, the Climate Variability and Predictability Program (CLIVAR) Repeat Hydrography/CO_2 Program (http://ushydro.ucsd.edu/) and Global Ocean Ship-Based Hydrographic Investigations Program (GO-SHIP; http://www.go-ship.org) began reoccupying several of the WOCE hydrographic lines [*Talley et al.*, 2016]. These observations target direct assessments of C_{anthro} uptake and storage in the ocean, which allow us to examine the changing role of the ocean in the global carbon cycle under climate change.

Despite being the largest ocean basin, the Pacific only stores about 18% of the global ocean inventory of anthropogenic CO_2 (C_{anthro}) [*Feely et al*., 2001]. The Pacific Ocean covers almost half of the total ocean area and therefore has the potential to experience significant changes in carbon cycling as climate continues to change. The Northeast Pacific, located at the end of the ocean meridional overturning circulation, is a region with particularly low concentrations of C_{anthro}. Both the lack of significant deep-water formation and slow meridional circulation limit the transport C_{anthro} into the ocean interior [*Reid*, 1997; *Sabine et al*., 2002; *Stuiver et al*., 1983]. As a result, the Pacific generally has much shallower C_{anthro} penetration and lower C_{anthro} storage compared to the Atlantic. In the North Atlantic, deep water formation and relatively fast ventilation allows anthropogenic CO_2 to almost reach the bottom (~5000 m) [*Gruber et al*., 1996; *Körtzinger et al*., 1999; *Wanninkhof and McGillis*, 1999].

Several categories of methods are used to estimate C_{anthro}, including back calculation methods to estimate ΔC^* [*Brewer*, 1978; *Chen and Millero*, 1979; *Gruber et al*., 1996], tracer-based methods [*Hall et al*., 2004; *Waugh et al*., 2006], and model-based approaches [*Khatiwala et al*., 2009; *Pardo et al*., 2014]. The various advantages and disadvantages to these methods are discussed in *Sabine and Tanhua* [2010]. In this paper, we use the extended multiple linear regression (eMLR) approach [*Friis et al*., 2005, *Tanhua et al*., 2007] to estimate the change in C_{anthro} between two data sets collected along the CLIVAR P17N transect in the Northeast Pacific. The eMLR method is well-suited to estimate changes in C_{anthro} for reoccupation of cruise transects over decadal scales, assuming that the relationships between the chosen regression parameters do not change substantially for the time period over which the eMLR is applied. An advantage of the eMLR method is that it does not require any assumptions of preindustrial concentrations. Recent studies in the South Pacific and Pacific sector of the Southern Ocean use the eMLR technique [*Waters et al*., 2011; *Williams et al*., 2015], but few studies have made DIC data-based estimates of the change in C_{anthro} storage in the Northeast Pacific with the exceptions of *Peng et al*. [2003] at 30°N, 152°W from 1973 to 1991 and *Sabine et al*. [2008] at P16N from 1991/1992 to 2006, from 200 to 1600 km west of the P17 transect.

The Northeast Pacific waters have naturally high dissolved inorganic carbon (DIC) concentrations, low pH, low buffering capacity, and a relatively shallow aragonite saturation horizon compared to other ocean basins. Even though this region does not currently hold a large amount of C_{anthro}, the system is already close to calcium carbonate undersaturation, which may have significant biological and ecological consequences. Therefore, studying how C_{anthro} storage changes in the Northeast Pacific is as important as understanding uptake in higher storage areas such as the North Atlantic. In this paper, we report the results from a 2012 cruise along a northern segment of the WOCE/CLIVAR P17 transect in the Northeast Pacific and evaluate changes in C_{anthro} and the carbonate system from 2001 to 2012. This is the first estimate of C_{anthro} using direct DIC measurements in the Northeast Pacific. We compare the decadal changes in C_{anthro} and carbonate chemistry at P17 with other Pacific regions and other ocean basins, and examine the corresponding mechanisms that may cause observed within-basin and between-basin differences. The storage rate estimate made from this study should be incorporated into the global inventory of C_{anthro} storage rate data to allow for further analysis of the uptake capacity of the ocean and its role in the global carbon cycle.

2. Data and Methods

2.1. Data Collection and Sample Analysis

Data were collected during a research cruise aboard the *R/V New Horizon* (cruise number NH1208) from 9 August to 18 September 2012 along a northern portion (33.5 – 50°N) of the WOCE/CLIVAR P17N cruise track (Figure 1). This cruise was part of a broader effort designed to investigate how the carbonate chemistry in the Atlantic and Pacific Oceans affects the abundance, distribution, species composition, shell condition and vertical migratory behavior of thecosomatous pteropods. Stations were at every 0.5° latitude and ~0.8° longitude from 50°N 150°W to 41°N 135°W and every 0.5° latitude along 135°W from 41°N to 33.5°N. Deep station casts were conducted every 2° latitude from 50 to 43°N, 1.5° latitude from 43 to 35.5°N and 1° latitude for the remaining stations. Sampling depths were chosen to match similar water column coverage from previous WOCE/CLIVAR cruises. Vertical sample spacing ranged from 20 m near the surface to 250 m below 1000 m.

A 24 position, 10 L bottle Rosette Niskin package equipped with a Conductivity-Temperature-Depth sensor (CTD, Seabird SBE 911plus) and a SBE43 dissolved oxygen (DO) sensor was used to collect discrete seawater

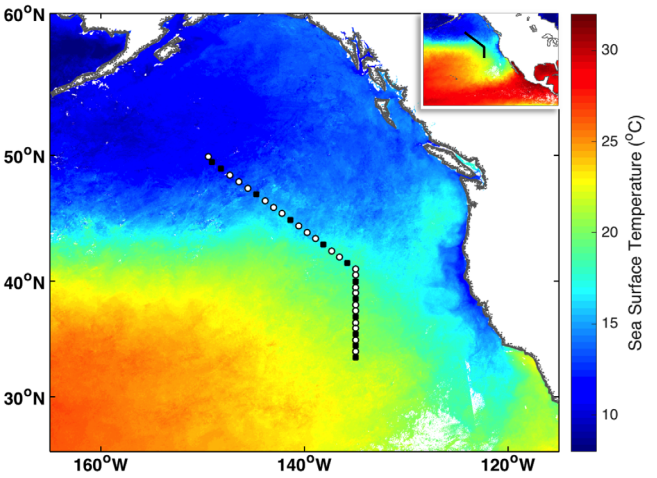

Figure 1. Northeast Pacific study region showing the segment of the P17N transect occupied by the present study (cruise NH1208) in 2012. For NH1208, there were 34 water-column sampling stations; 22 (white circles) were sampled to 1000 m at 15 depths while the rest (black squares) were sampled to 3000 m at 24 depths. Color scale shows sea surface temperature from a 1 month satellite composite of Aqua MODIS data centered at 16 August 2012.

samples for analysis of total dissolved inorganic carbon (DIC), total alkalinity (TA), pH, DO, nutrients (nitrate, phosphate, and silicate), and salinity. Seawater samples were collected for pH, DIC, TA, and nutrients at all 34 stations for all sampling depths. Salinity and DO samples were collected at all stations at every third depth for calibrations of the conductivity and DO sensors on the CTD Rosette. Samples for DO were collected first from the Niskin bottles, followed by pH, DIC/TA (in the same bottle), nutrients, and salinity. Standard protocols were followed for sampling procedures [*Dickson et al*., 2007]. DIC and TA samples were collected into 250 ml Pyrex borosilicate bottles after being filtered with a 0.45 μm in-line capsule filter (Farrwest Environmental Supply, Texas). Each sample was poisoned with 100 μL of a saturated mercuric chloride solution for preservation [*Dickson et al*., 2007] and sealed with a ground-glass stopper coated with APIEZON®-L grease and was secured with a rubber band applied to the bottle top.

DIC was analyzed using an Apollo SciTech DIC auto-analyzer (Model AS-C3), which uses a nondispersive infrared (NDIR) method. The sample is acidified with a 10% phosphoric acid in 10% sodium chloride solution, and CO_2 is purged with high purity nitrogen gas and measured by a LI-COR 7000 infrared analyzer. Certified Reference Material (CRM) from Dr. A. Dickson at Scripps Institution of Oceanography was used to calibrate the DIC auto-analyzer at least once daily. In addition, CRM was measured as a sample every few hours to gauge and correct any potential drift. The precision and accuracy of the instrument was $\sim \pm 2.0$ μmol kg^{-1}. The average absolute difference of duplicates was 5.4 ± 4.5 μmol kg^{-1} (N=29). The larger standard deviation of duplicates may be a result of sampling, storage, or other sources of error.

TA was measured with an Apollo SciTech alkalinity auto-titrator (Model AS-ALK2), a Ross combination pH electrode and a pH meter (ORION 3 Star) to perform a modified Gran titration [*Wang and Cai*, 2004]. The electrode and concentration of hydrochloric acid was calibrated every day. The CRMs were also measured as samples every few hours to correct any potential small drift. The average absolute difference of duplicate samples was 2.7 ± 2.1 μmol kg^{-1} (N=28), which is similar to the accuracy and precision of the instrument, about ± 2.0 μmol kg^{-1}.

Seawater pH samples were collected directly into 10 cm cylindrical optical cells via silicone tubing and thermostated to 25.0 ± 0.1°C for at least an hour before measurement. Samples were analyzed using an Agilent 8453 UV-VIS spectrophotometer and *meta*-cresol purple (*m*-CP) as the indicator [*Dickson et al*., 2007]. Sample pH was measured on the total scale. Measurements of pH were corrected for indicator perturbation and indicator impurity [*Clayton and Byrne*, 1993; *Dickson et al*., 2007; *Liu et al*., 2011; *Yao et al*., 2007]. The average of combined corrections was 0.0026 ± 0.0046. The average absolute difference of duplicates (N=28) was 0.0014 ± 0.0010, which is similar to the instrument accuracy and precision of 0.002 and 0.001, respectively.

The nutrient samples were filtered through 0.2 μm filters, collected into vials that had been cleaned with 10% hydrochloric acid and were immediately frozen after collection. Samples were analyzed at the University of California at Santa Barbara Marine Science Institute. Nutrient data from NH1208 were found to have relatively larger scatter than the previous P17N cruise data. This may be due to storage issues that involved freezing and possible melting of samples. Further details regarding analysis procedures for DO and salinity can be found in the supporting information (SI).

Table 1. PACIFICA Recommended Adjustments for CLIVAR P17N 2001 Are Shown Here Along With Deep Isopycnal Crossover Results for NH1208 2012 Cruise Adjusted to the CLIVAR 2001 PACIFICA-Corrected Data[a]

	Salinity	Oxygen	Nitrate	Silicate	Phosphate	DIC	TA
CLIVAR 2001	0	1	1	1.048	1	−4	8
NH1208 2012	0	0.955	1	1.032	1.021	11	10

[a]Salinity, DIC, and TA factors are additive, while oxygen, nitrate, phosphate, and silicate factors are multiplicative. Units for all parameters are in μmol kg^{-1} except for salinity, which is measured on the practical salinity scale.

Bottle samples were assigned WOCE quality flags. Property-property plots were also examined to check for any aberrant data points. Samples in the near surface were allowed more variability in flagging. Data below 1000 m were also compared against 2001 CLIVAR data and strong deviations were noted.

2.2. Internal Consistency

The seawater inorganic carbon system can be described by four measurable parameters: DIC, TA, pH and fugacity of CO_2 or fCO_2. Any pair of carbon parameters can be used to define the remaining parameters based on CO_2 equilibrium relationships. To test for internal consistency within the measured DIC, TA, and pH data, carbonate system parameters were calculated using the CO2SYS program by *Pierrot et al*. [2006] with constants from *Mehrbach et al*. [1973] as refit by *Dickson and Millero* [1987]. Crossover-corrected DIC (details described in section 2.4), TA, and pH data were used in CO2SYS calculations to compare with measured values in order to determine offsets and outliers. In this case, DIC was calculated from measured TA and pH to compare with measured DIC values. The mean residual (calculated – measured value) for DIC (N=562) was 0.5 ± 9.0 μmol kg^{-1} (one standard deviation). There was good agreement over the entire water column and residuals were randomly distributed, suggesting there were no significant systematic errors in the data. The mean difference was within required accuracies for C_{anthro} calculation, while the variation of this data set was somewhat higher than the previous CLIVAR P17N DIC data, which had an internal consistency for DIC of 3.2 ± 6.6 μmol kg^{-1}. This had a limited effect on C_{anthro} estimates, since the eMLR method should remove most of the random scattering in the data set by comparing estimated means [*Tanhua et al*., 2007; *Wanninkhof et al*., 2010].

2.3. Selection of Previous CLIVAR Data

The NH1208 cruise occupied a portion of the CLIVAR P17N cruise track, which was previously occupied in 25 July to 28 August 2001 by a CLIVAR cruise. For the 2001 CLIVAR cruise (data from CLIVAR and Carbon Hydrographic Office (CCHDO) http://cchdo.ucsd.edu/cruise/49NZ200107_1), there were 78 stations. Discrete samples were taken for salinity, DO, nutrients, DIC, and TA. Salinity, DO, and nutrients were taken at every station for every depth. pH, DIC, and TA samples were taken at every other station. The data from the stations that overlap in latitude for the two cruises were used to quantify the total changes of seawater chemistry over the decade. The overlapping sections include stations 1–32 for NH1208, corresponding to stations 28–73 for CLIVAR. CLIVAR sampled every 0.5° latitude from 33.5–41°N at 135°W for 36 depths to 4000–5000 m and then every 0.3° latitude, 0.5° longitude from 41–50°N. The duplicate DIC, TA, and pH samples were within acceptable limits for accuracy and precision. CLIVAR data were not seasonally corrected for the eMLR analysis because of similar timings between the 2001 (July–August) and 2012 (August–September) cruises. The CLIVAR carbonate data quality was also confirmed by Certified Reference Materials [*Dickson*, 2001; *Feely et al*., 2001].

2.4. Deep Crossover Analysis

To remove biases between the 2012 and 2001 data sets, the deep isopycnal crossover analysis method [*Lamb et al*., 2002] was used at the overlapping stations. This method assumes that Pacific Deep Water with a residence time of ~500 years [*Stuiver et al*., 1983] does not experience significant changes over decadal timescales. Shallow depths are subject to changes due to seasonal variability of biological processes and penetration of C_{anthro}, which can vary the relationships between carbon parameters over different periods of time. For the CLIVAR occupation, crossover analyses have already been conducted and adjustments have been made according to PACIFic ocean Interior CArbon (PACIFICA) [*Suzuki et al*., 2013] (Table 1). PACIFICA adjustments are recommended based on calibration procedures, CRM analyses, precision of replicates, deep-water crossover analyses and internal consistency. Estimated accuracy after PACIFICA adjustments was ± 4 μmol kg^{-1} for DIC and ± 6 μmol kg^{-1} for TA.

Table 2. Coefficients Used for the DIC (μmol kg^{-1}) eMLR Analysis of 2001 CLIVAR and 2012 NH1208 Cruises

	INTERCEPT	AOU (μmol kg^{-1})	S (PSS-78)	θ (°C)	Si (μmol kg^{-1})	N	RMSE	R^2
2001	892.8 ± 28.6	0.67 ± 0.01	36.25 ± 0.78	−7.58 ± 0.18	0.36 ± 0.02	278	2.9	0.9993
2012	797.6 ± 102.5	0.64 ± 0.02	39.96 ± 3.15	−9.22 ± 0.46	0.23 ± 0.04	315	10.0	0.9922

To make adjustments to the NH1208 2012 cruise data, data from >2000 m were used for the crossover analysis. It should be noted that NH1208 has fewer data points below 2000 m than CLIVAR 2001, which might affect comparison statistics. Salinity and oxygen, along with carbonate system parameters and nutrients were compared using potential density referenced to 3000 dbar (σ_3). The data from each of the CLIVAR and NH1208 cruise occupations of this portion of P17N (2001 and 2012) were plotted against σ_3 and fit by a second-order polynomial (supporting information Figure S1). Only data with acceptable quality flags were used in the crossover analysis. Oxygen, silicate, phosphate, DIC, and TA required corrections (Table 1).

2.5. Extended Multiple Linear Regression

The eMLR method is a derivative of the MLR introduced by *Wallace* [1995] that develops an empirical relationship to characterize DIC variability using chemical and hydrographic parameters [*Friis et al*., 2005]. The original MLR method uses data sets from the same region from two different time periods and derives a MLR for one period, usually the earlier period. Those coefficients are applied to data from the later period and then the difference between the calculated and observed DIC for the later period is taken as the change in anthropogenic CO_2 between the two time periods, ΔC_{anthro}. In the eMLR method, MLRs are created separately for two periods using the same sets of regression model variables, and the difference of the coefficients applied to data from one of the time periods, usually the later period, is used to calculate ΔC_{anthro}.

The eMLR was conducted on the water column from 100 to 1000 m depth and the entire transect as a whole. The eMLR was only applied to data from 100 to 1000 m due to the fewer number of data points below 1000 m for the 2012 NH1208 cruise. The top 100 m of the water column was not included in the fit to exclude apparent trends due to complex, seasonally varying surface processes in the mixed layer, such as high biological production and air-sea exchange, which may affect eMLR results. Surface values (0–100 m) were estimated based on the assumption that fCO_2 in the surface water changes at the same rate as fCO_2 in the atmosphere [*Sabine et al*., 2008; *Waters et al*., 2011].

The eMLR was not separated by potential density bins or by latitudinal ranges due to the limited data availability caused by removing flagged nutrient data as mentioned previously. Calculating MLRs by potential density bins is useful in removing errors introduced by isopycnal heave at seasonal and decadal scales [*Doney et al.,* 2007; *Levine et al*., 2008; *Wanninkhof et al*., 2010]. However, our analysis did not show significantly large errors by applying one MLR to the entire transect for both years.

The coefficients of the eMLR regressions on DIC for the two time periods are shown in Table 2. The best set of parameters to characterize DIC was apparent oxygen utilization (AOU), salinity (S), potential temperature (θ), and silicate (Si). This set of parameters was chosen based on reducing the error of the fit while taking into consideration data quality. AOU, salinity, and potential temperature were tested in models with one or a combination of nutrients. Among the nutrients, silicate was found to improve the fit the most while adding phosphate and/or nitrate led to minimal improvement. The RMSE of 10.0 μmol kg^{-1} is similar to the uncertainty in the internal consistency calculations (9.1 μmol kg^{-1}). No significant systematic trends were found when plotting residuals (model-observation) against potential density, latitude, and depth (supporting information Figure S2).

Total alkalinity was not included in the MLR because it did not significantly improve the MLR fit and there was a co-linearity found between TA and salinity. In addition, contribution to changes in DIC due to calcium carbonate precipitation or dissolution were negligible in that there was no significant difference in salinity-normalized total alkalinity compared on isopycnals between the two cruises.

3. Results

3.1. Latitudinal Distribution of Geochemical Features Along P17N

The salinity and density fields show strong upper-ocean vertical stratification in the northern part of the transect in the subpolar gyre where colder, fresher water is dominant in the surface (Figure 2a). The transition zone between the subpolar and subtropical gyres can be defined by the outcrops of isohaline 33.0 and 33.8 [*Roden*, 1991], which are found here at 42°N and 34°N, respectively. This indicates that the 2012 cruise did not extend into the waters of the subtropical gyre. Depth profiles of salinity show only subpolar gyre and transition zone salinity structure, with low salinity in the surface that increases with depth. Subtropical gyre salinity depth profiles have high salinity in surface waters with a clear presence of the North Pacific Intermediate Water (NPIW) salinity minimum and slight increase of salinity with depth below [*Talley*, 1993], neither of which are seen in Figure 2a. The potential density contours shown in Figure 2 shoal from the southern part of the transect toward the northern part. The shallow isopycnals in the northern latitudes are caused by wind-driven upwelling where there is outcropping of the isopycnals. It is evident that water movement is primarily along isopycnals [*Gruber et al*., 1996; *Iselin*, 1939; *Quay et al*., 2007] as shown by horizontal distribution patterns of all parameters in Figure 2 that generally follow the isopycnals.

AOU is mostly negative near the surface along P17N (Figure 2b), indicating oxygen supersaturation due to summer heating and greater net community production [*Broecker and Peng*, 1982; *Shulenberger and Reid*, 1981]. In the southern part of P17N, there is an area of AOU of 250 μmol kg^{-1} and greater between 500 and 1500 m that gradually expands to 350–2000 m at the northern part of the transect. This AOU horizon corresponds to an oxygen concentration of ~50 μmol kg^{-1}, used here as the upper limit definition of an oxygen minimum zone (OMZ). A combination of weak ventilation and high oxygen utilization allows for the formation of OMZs, an area that is also accompanied by high DIC.

The vertical structure of DIC shows low concentrations in surface waters and increasing concentrations with depth (Figure 2c). The lowest DIC values of <2000 μmol kg^{-1} in the surface waters are partially due to elevated biological productivity converting DIC into organic carbon that subsequently sinks from the upper ocean. Surface DIC concentration is slightly higher in the colder, fresher water of the northern latitudes than the southern part of the transect. Additionally, there is shoaling of high DIC water at depth along isopycnals in the northern latitudes due to upwelling and outcropping of old and deep water. The middepth water in this region is especially rich in DIC and nutrients due to the accumulation of products from remineralization. The distribution patterns of AOU and DIC are correlated because similar processes such as circulation, air-sea exchange, solubility, and biological activities modulate both AOU and DIC.

The ability of seawater to buffer CO_2 entering the ocean can be described by the Revelle Factor $\left(RF = \frac{\partial \ln [CO_2]}{\partial \ln DIC}\right)$ [*Broecker et al*., 1979; *Egleston et al*., 2010; *Revelle and Suess*, 1957]. A lower RF represents a larger buffer capacity for a parcel of water. An increase in pCO_2 or DIC for a water parcel tends to increase the parcel's Revelle Factor and make it less able to absorb more CO_2. Currently, the RF across ocean basins varies between 9 and 15 and has increased by approximately one unit since preindustrial times [*Egleston et al*., 2010; *Sabine et al*., 2004]. In general, the Northeast Pacific region has a higher than average RF within the mixing zone because these older waters have higher DIC and lower pH. Figure 2d shows that the surface RF varied from 11 to 13, with the higher surface values found in the northern part of the transect, where the water is the coldest and freshest. For a given increase of surface pCO_2, the southern part of the transect would absorb more CO_2 and thus experience a larger increase in DIC than the northern part, assuming other system factors remain constant.

Physical, biological, and anthropogenic changes along P17N can be examined by directly subtracting gridded parameters of 2001 from 2012. Changes in physical processes, such as circulation and frontal movement can cause changes in salinity, AOU, and DIC. AOU and DIC can also be influenced by ventilation and biological processes. In addition, DIC changes can be attributed to invasion of anthropogenic CO_2. Between 2001 and 2012, changes in salinity along P17N are almost completely confined to the upper 300 m (Figure 3a). A salinity increase of ~0.4 units is found from 125 to 300 m from 36 to 48.5°N, with an especially large increase up to 0.6 units in the top 50 m from 37.5 to 39.5°N. There is fresher water in the subpolar gyre as shown by the decrease in salinity of 0.1–0.3 units near 50°N. The changes in surface salinity along P17N agree with the overall reported surface ocean trends from 1950 to 2008, where evaporation-dominated areas experienced salinity increases and precipitation-dominated areas experienced salinity

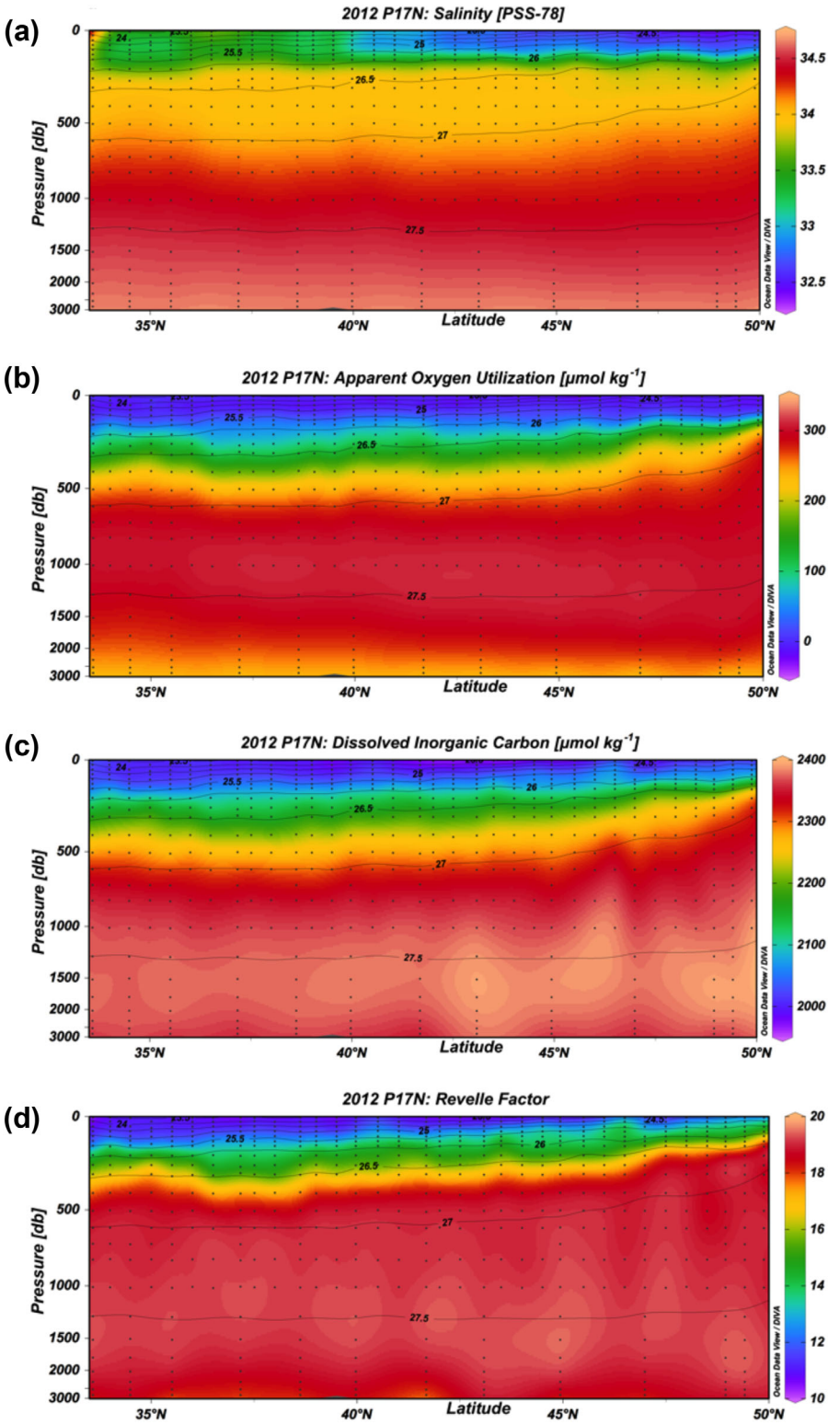

Figure 2. (a–d) Latitudinal sections from the 2012 occupation of P17N for salinity, AOU, DIC, and Revelle Factor (calculated from DIC and TA) overlaid with potential density contours. The sections are gridded on 1° by 50 m grids with Data-Interpolating Variational Analysis (DIVA) software in Ocean Data View [*Schlitzer*, 2015].

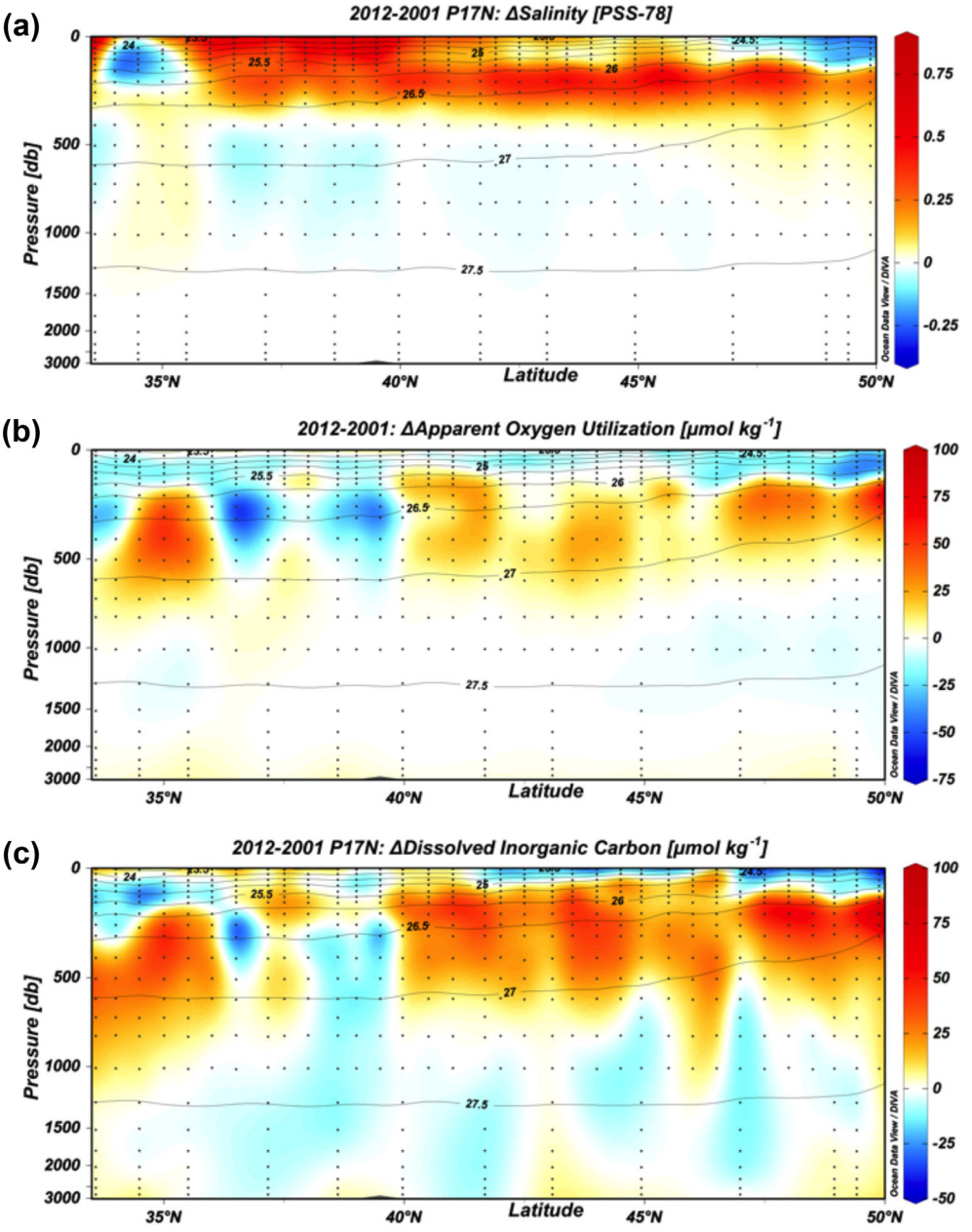

Figure 3. (a–c) Differences between repeat occupations of P17N from 2001 CLIVAR and 2012 NH1208 for salinity, AOU, and DIC overlaid with potential density contour lines.

decreases [*Durack and Wijffels*, 2010]. Multiple studies have reported freshening in the North Pacific Ocean, primarily in the upper 100 m. The pattern differs in shallow subsurface waters. *Boyer et al.* [2005] and *Durack and Wijffels* [2010] both find a salinity increase in subpolar North Pacific at 50°N at 150 m, which agree with the subsurface salinity increase along P17N.

Changes in AOU are seen from the surface to ~600 m. In the upper 100 m, there are mostly decreases of 10–20 μmol kg^{-1} over the transect with a more intense area of decrease up to 40 μmol kg^{-1} near 50°N (Figure 3b). For 100–600 m, the overall pattern in ΔAOU shows an increase in concentrations from 2001 to 2012. Since the 1970s, a decrease in overturning circulation has been reported in the subpolar North Pacific [*Deutsch et al.*, 2006; *McPhaden and Zhang*, 2002; *Mecking et al.*, 2008; *Sabine et al.*, 2008]. Reduced circulation in addition to warming (data not shown) would lead to greater stratification that would result in deoxygenation, an increase in AOU, and an intensification as well as expansion of the OMZ. Most of the large

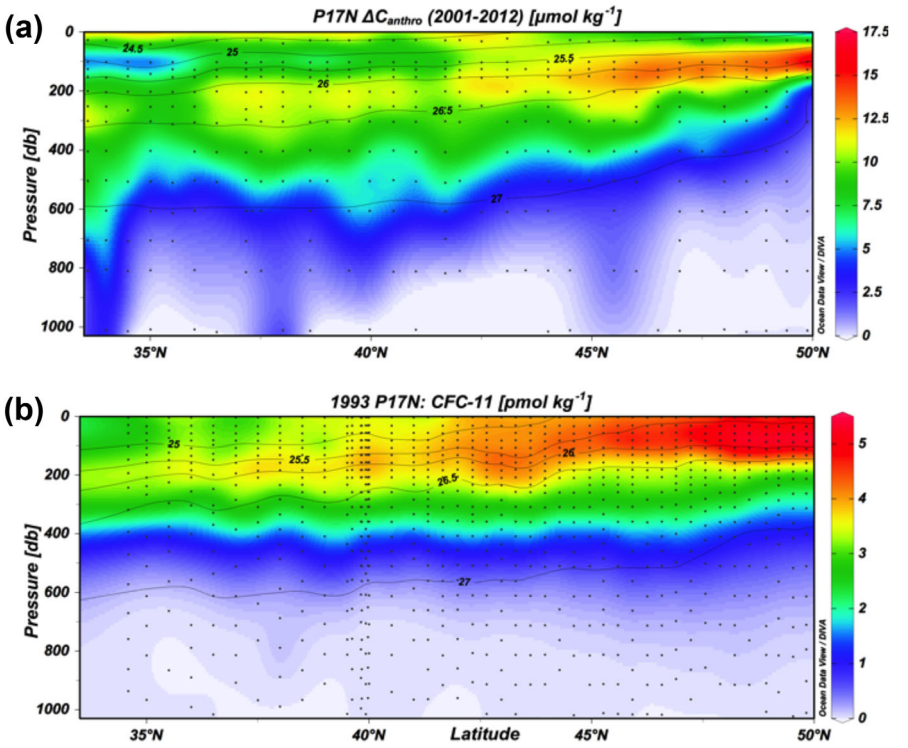

Figure 4. (a) Cross-sectional plot of eMLR calculated change in anthropogenic CO_2 from 2001 to 2012 along P17N with potential density contour lines. Negative ΔC_{anthro} are displayed as zero. (b) Cross-sectional plot of WOCE 1993 CFC-11 concentrations across P17.

AOU changes are seen between the 26 and 27 kg m^{-3} isopycnals. This is consistent with data along the 26.6 kg m^{-3} isopycnal, which is the densest isopycnal to outcrop in the open North Pacific in climatological data, [*Mecking et al*., 2008]. It is the upper-most isopycnal involved in the formation of NPIW and serves as an interface between ventilated waters and indirectly or nonlocally ventilated deeper waters. By averaging ΔAOU for isopycnals 26.55–26.65 kg m^{-3}, centered on 26.6 kg m^{-3} (Figure 3b), the mean AOU increase from 2001 to 2012 was was $+13.4 \pm 15.5$ μmol kg^{-1}. Changes in AOU and *in situ* O_2 should be similar in magnitude though opposite in sign because potential temperature and salinity variations are relatively small along isopycnals [*Mecking et al*., 2008]. The mean deoxygenation between 2001 and 2012 calculated from *in situ* dissolved O_2 concentration changes was -12.8 ± 13.9 μmol kg^{-1} centered on the same isopycnal 26.6 kg m^{-3} similar to calculated AOU changes. Mean ΔAOU and ΔO_2 are also comparable to an expected deoxygenation of -7.6 ± 0.1 μmol kg^{-1}, based on the rate of 0.68–0.70 μmol kg^{-1} yr^{-1} found on isopycnals 26.5 and 26.7 kg m^{-3} reported at Ocean Station Papa (50°N, 145°W) [*Falkowski et al*., 2011; *Whitney et al*., 2007].

Changes in DIC are seen throughout the whole water column. Down to 600m, ΔDIC patterns are similar in sign and somewhat larger in magnitude to those of ΔAOU, with additional unmatched temporal differences in DIC below 600 m. The similarities between the ΔDIC and ΔAOU distributions is expected due to remineralization and circulation processes that affect the distribution of both parameters similarly, leading to covarying patterns between the two (Figures 3b and 3c). The difference between the ΔDIC and ΔAOU distributions is likely attributed to C_{anthro} affecting DIC but not AOU. However, it seems that the factors affecting AOU changes account for a majority of the DIC changes, which agrees with [*Sabine et al*., 2008] finding that changes in AOU account for 80% of total DIC change in the North Pacific.

3.2. Distribution of Decadal Changes of Anthropogenic Carbon Dioxide Along P17N

From 2001 to 2012, across the P17N transect, ΔC_{anthro} values at the surface have a range of 7 – 11 μmol kg^{-1} (Figure 4). Such a range is similar to an expected 13–17 μmol kg^{-1} increase in surface water DIC based on a growth rate of 1.36 ± 0.16 μatm yr^{-1} in surface seawater pCO_2 measured at Station P (50°N, 145°W) [*Wong et al*., 2010]. The coarse transition between the top 100 m and the rest of the water column is due to separate

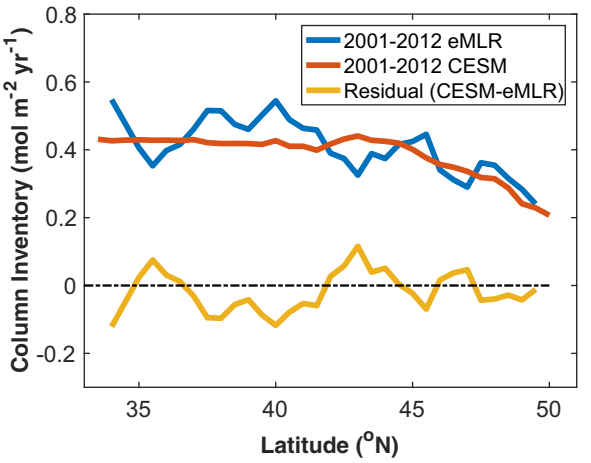

Figure 5. Change in column inventory of C_{anthro} between 2001 and 2012 binned to 1° latitude resolution. The eMLR results (blue) are compared to those estimated using a community ecosystem model (CESM) (red) [*Doney et al.*, 2009a, 2009b]. The residual between the two models is plotted in yellow.

treatment of the surface layer as mentioned previously. The penetration depth of ΔC_{anthro}, roughly defined by the $+2.5$ μmol kg^{-1} isoline, is at approximately 700–1000 m in the southern part of the transect, shoaling to approximately 400 m in the subpolar gyre at 50°N, likely reflecting prevailing upwelling patterns that compress the anthropogenic signal near the surface ocean. Because there is no deep-water formation in the Northeast Pacific, C_{anthro} does not penetrate into the deep ocean in this region. In the upper thermocline (~300 m), ΔC_{anthro} decreases equatorward along isopycnal surfaces, consistent with thermocline ventilation pathways.

The distribution pattern of ΔC_{anthro} can be partially verified by comparison to measured anthropogenic chlorofluorocarbon (CFC), trichlorofluoromethane (CFC-11), from a previous WOCE cruise in 1993 along P17N (Figure 4b). The CFC data show similar patterns to the ΔC_{anthro} in terms of the north-south gradients along isopycnal surfaces in the upper 300 m. Vertically, CFC penetration reaches ~400 m and is almost uniform with latitude, except at the very northern part of the transect. Considering the different input histories and chemical properties between anthropogenic CO_2 and CFCs and the different time frame between Figures 4a and 4b, their difference in distribution patterns is expected. Nevertheless, the similarity of the distribution between ΔC_{anthro} and CFCs suggests the results of the eMLR-derived ΔC_{anthro} in this study are reasonable.

3.3. Change in Anthropogenic CO_2 Water Column Inventory

Using C_{anthro} surface values (0–100 m) based on the assumption of surface ocean-atmosphere equilibrium, the average increase in ΔC_{anthro} column inventory across P17N based on the eMLR analysis was $+0.41 \pm 0.12$ (1σ) mol m^{-2} yr^{-1}. There are at least two other methods that can be used to estimate surface layer ΔC_{anthro}, one of which is to include surface values in the eMLR [*Friis et al.*, 2005; *Wanninkhof et al.*, 2010]. While we did not include the surface values in our eMLR, we applied eMLR coefficients to the surface data to estimate surface ΔC_{anthro} calculated an average column inventory of $+0.39 \pm 0.09$ mol m^{-2} yr^{-1}. Secondly, if eMLR-calculated ΔC_{anthro} values at 100 m were extrapolated to the surface [*Brown et al.*, 2010], the column inventory would be $+0.43 \pm 0.12$ mol m^{-2} yr^{-1}. Therefore, using different methods of estimating the ΔC_{anthro} surface values do not significantly affect the end result. To calculate the column inventory, negative ΔC_{anthro} values were set to zero. Depth profiles were interpolated using a piecewise cubic hermite interpolation [*Tanhua et al.*, 2007, 2010]. Then with trapezoidal integration, the column-integrated ΔC_{anthro} was calculated at each station. Stations that had insufficient data (less than two depths of data) were not included. The uncertainty reported here is the standard deviation of the average change in column inventory across P17N and thus includes regional variations. The storage rate across the transect shows a general decrease from $+0.55$ mol C m^{-2} yr^{-1} at 34°N to $+0.20$ mol C m^{-2} yr^{-1} at 50°N with significant latitudinal variability (Figure 5). As the high latitude waters experience an upwelling regime with surface divergence and lateral transport of C_{anthro} in the subpolar gyre, there is expected lower accumulation of C_{anthro} near the surface at the northern stations [*Sabine et al.*, 2004]. The higher change in column inventory in the lower latitudes transitioning toward the subtropical surface waters, similarly, is consistent with a convergent, downwelling regime where anthropogenic carbon and CFCs are transported downward along isopycnal surfaces into the ocean interior.

The storage rate calculated using eMLR is similar to simulation results from the Community Earth System Model (CESM) [*Doney et al.*, 2009a, 2009b]. The storage rate from the CESM ranges from $+0.21$ to $+0.43$ with an average rate of $+0.38 \pm 0.06$ mol m^{-2} yr^{-1}. The average storage rate calculated by the two methods agree within uncertainties and follow a similar latitudinal pattern with higher rates in the southern half of the transect decreasing to lower rates in the northern half of the transect. The eMLR results show higher

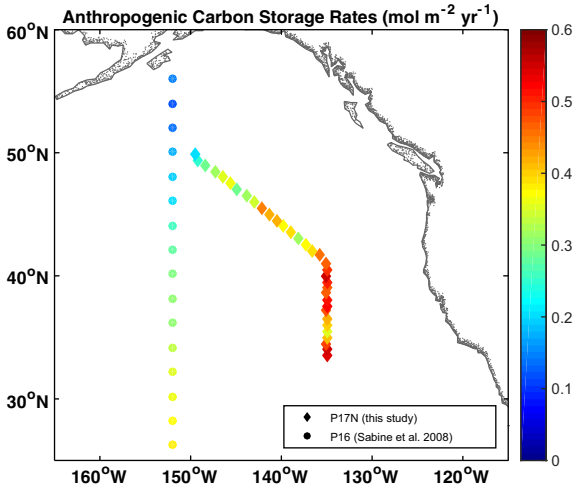

Figure 6. Comparison of the ΔC_{anthro} storage rates between the P17N transect (2001–2012) and the P16 transect (1991/1992–2006) [*Sabine et al.*, 2008].

degree of variation along the transect. The overall agreement between these two different methods suggests that the results from the eMLR method are robust.

4. Discussion

4.1. Anthropogenic Carbon Storage Rates

Two other observational, DIC data-based studies have estimated ΔC_{anthro} near P17N. *Peng et al.* [2003] used a MLR method at 30°N, 152°W and data from Geochemical Ocean Section Study (GEOSECS) 1973 and WOCE/JGOFS 1991 to estimate an average rate of 1.3 ± 0.5 mol C m^{-2} yr^{-1}. *Sabine et al.* [2008] estimated an average rate of 0.25 mol m^{-2} yr^{-1} along the WOCE/CLIVAR P16N transect (0–56°N, 152°W), west of P17N, between 1991/1992 and 2006 based on an eMLR method (Figure 6). The earlier estimate by *Peng et al.* [2003] is likely to be an overestimate due to systematic biases in the GEOSECS DIC data [*Quay et al.*, 2007; *Sabine and Tanhua*, 2010].

Differences in the application of the eMLR may partially explain the differences in the estimated ΔC_{anthro} between P16 and P17. The P16 study [*Sabine et al.*, 2008] was conducted on data from 1991/1992 and 2006 using a somewhat different eMLR approach. They first calculated total DIC change (ΔC_{total}) and carbon change calculated from AOU (ΔC_{AOU}) using separate eMLRs but with the same regression parameters: potential temperature, salinity, silicate, and phosphate. Then they computed ΔC_{anthro} by correcting the ΔC_{total} for ΔC_{AOU}, assuming an organic matter C:O_2 stoichiometry of 117/170 [*Anderson and Sarmiento*, 1994], where the AOU correction reduces the ΔC_{total} substantially, by up to 80%. *Sabine et al.* [2008] argue that the ΔAOU patterns primarily reflect variations in circulation rather than export, but to some extent any resulting changes in remineralized carbon in the subsurface should already be captured by the two eMLRs through the variations of phosphate that contribute to both the AOU and total DIC regressions. Here we used AOU as an eMLR regression parameter for the P17N ΔC_{anthro}, in part because of the poor quality of the phosphate data from NH1208. Therefore, a direct comparison to the Sabine et al. two-step eMLR approach is not possible. Note, though, that the small-scale patterns in ΔAOU and ΔDIC (Figures 3b and 3c) are largely removed from ΔC_{anthro} (Figure 4a), suggesting that to some degree AOU trends are adequately captured in our approach.

With these caveats in mind, Figure 6 shows a comparison from this study to the results from *Sabine et al.* [2008] for P16N. At 50°N, where the two transects are closest, there is similarity between the two storage rates at 0.20 and 0.18 mol m^{-2} yr^{-1} for P17 and P16, respectively. As the transects separate, so do the estimated storage rates, with the P17 storage rates increasing to 0.54 mol m^{-2} yr^{-1} at 33.5°N, while for P16 the rate is ~0.34 mol m^{-2} yr^{-1}. Given the uncertainty associated with P16 and P17 calculations of 0.2 and 0.12 mol m^{-2} yr^{-1}, respectively, these differences are likely not statistically significant. Future studies could delve deeper into these technique driven differences. Besides methodological reasons that could cause these differences, P17 is further east than P16 by 2–17° in longitude and is subject to slightly different currents and water masses. Comparing these rates to those in the Northwest Pacific, average storage rates are reported as 0.4 ± 0.1 – 0.5 ± 0.2 mol m^{-2} yr^{-1} [*Murata et al.*, 2009; *Wakita et al.*, 2013], which are not significantly different from the P16N and P17N values [*Sabine et al.*, 2002, 2008]. Further observation and analysis are needed to fully understand the spatial distribution of ΔC_{anthro} across the Pacific.

Estimated C_{anthro} storage rates in the Pacific are lower than the rates at similar latitudes in the North Atlantic. North Atlantic storage rates ranging from 0.6 to 2.2 mol m^{-2} yr^{-1} are consistent with the higher cumulative C_{anthro} inventory for the basin [*Friis et al.*, 2005; *Quay et al.*, 2007; *Sabine and Tanhua*, 2010; *Tanhua et al.*, 2007]. The average storage rate across P17N of 0.41 ± 0.12 mol m^{-2} yr^{-1} agrees within uncertainty to

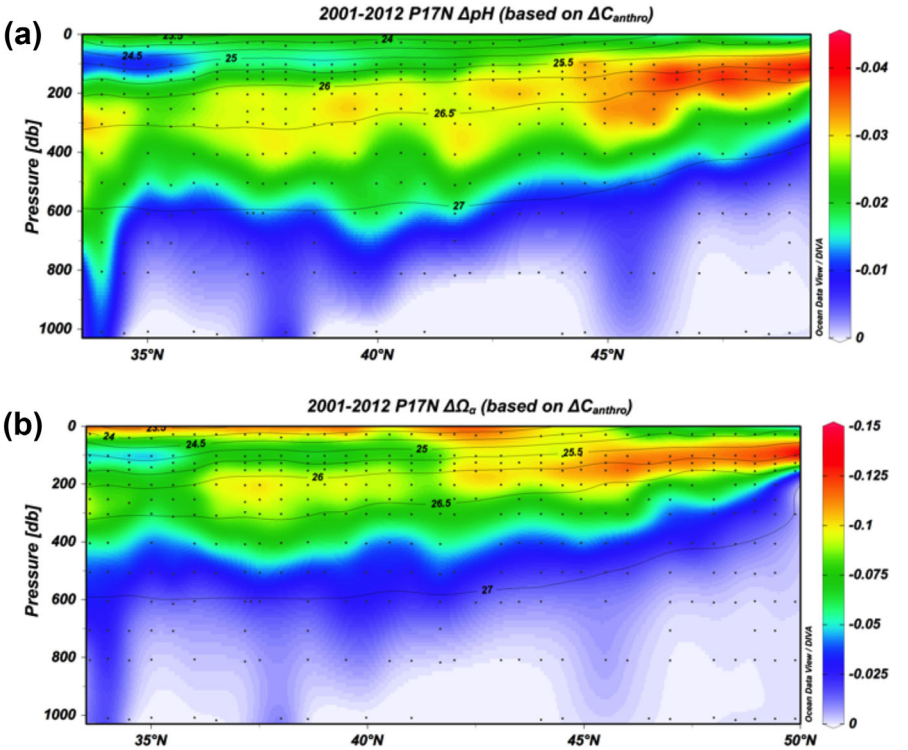

Figure 7. Latitudinal distribution of change in (a) pH and (b) aragonite saturation state due to ΔC_{anthro} along the P17 transect between 2001 and 2012 with potential density contour lines.

0.63 ± 0.16 mol m^{-2} yr^{-1} estimated from *Quay et al.* [2007] for the entire North Atlantic. However, taking a closer look at specific latitudes that overlap with our P17N transect, the P17N storage rate is significantly lower than 1.2 ± 0.3 and 2.2 ± 0.7 mol m^{-2} yr^{-1}, found in the Atlantic at 20–40°N and 40–65°N, respectively [*Friis et al.*, 2005; *Tanhua et al.*, 2007]. The high inventory and storage rate are mainly the result of deep-water formation in the North Atlantic, which drives the transport of C_{anthro} into the ocean interior [*Khatiwala et al.*, 2013; *Mikaloff Fletcher et al.*, 2006]. With no deep-water formation and upwelling in the Northeast Pacific, C_{anthro} penetration and accumulation is limited.

4.2. Anthropogenic CO_2 Effects on Carbonate Chemistry

Since the beginning of the industrial era, atmospheric CO_2 has increased from ~280 ppm to over 400 ppm (http://www.esrl.noaa.gov/gmd/ccgg/trends/weekly.html). By 2100, atmospheric CO_2 levels are projected to reach near 1000 ppm under a business-as-usual scenario [IPCC, 2014]. This could lead to irreversible damage to Earth's marine ecosystems through a myriad of effects, which can be partially gauged by monitoring of the rate of ocean acidification and the shoaling rate of the aragonite saturation horizon ($\Omega_a = 1$).

To evaluate the effect of the increase in C_{anthro} on the carbonate system of this region, the results from the eMLR were used to calculate changes in pH (ΔpH) and aragonite saturation state ($\Delta\Omega_a$) as a result of ΔC_{anthro}. pH and Ω_a were first calculated for 2012, using measured DIC and TA. To calculate pH and Ω_a for 2001, an expected 2001 DIC value was obtained by subtracting eMLR-calculated ΔC_{anthro} from the 2012 DIC value. This expected DIC was then used with the 2012 TA value to calculate expected pH and Ω_a. It is assumed that any TA change between the 2001 and 2012 is due to natural variability, therefore, using TA from 2012 for 2001 calculations should remove natural variability of TA and the change in pH and Ω_a between 2001 and 2012 would be solely due to increase in C_{anthro}.

The decadal change in pH (ΔpH, Figure 7a) or the ocean acidification rate in this region has similar patterns to the ΔC_{anthro}, as ΔC_{anthro} is the sole driving force for the ocean acidification rate calculated here. The estimated pH decrease can be translated to an acidification rate of 0.0008–0.004 pH units yr^{-1} in the upper 100 m, with an average rate of ~0.002 ± 0.0009 pH units per year. Such rates are slightly higher than the

rates of 0.0016 ± 0.0001 – 0.0018 ± 0.0001 pH units per year estimated for HOT, Station ALOHA, and P16N in the North Pacific [*Bates et al*., 2014; *Byrne et al*., 2010; *Dore et al*., 2009; *Takahashi et al*., 2014]. Ocean acidification in the Northwest Pacific has been estimated to occur at a rate of 0.0015 ± 0.0005 – 0.002 ± 0.0007 units per year [*Ishii et al*., 2011; *Midorikawa et al*., 2010]. These differences in ocean acidification rates are consistent with those differences in ΔC_{anthro} previously described.

The distribution of $\Delta\Omega_a$ also follows the pattern of ocean acidification rates (Figure 7). The decrease of Ω_a due to increases in C_{anthro} has resulted in a shoaling of the aragonite saturation horizon ($\Omega_a = 1$) by 10 – 35 m with an average of ~19.6 m over 11 years, or ~1.8 ± 0.4 m yr^{-1}. At 50°N, $\Omega_a = 1$ is near 125 m, the shallowest depth over the transect. At this rate, the entire water column in the northern part of the P17N will become undersaturated in 50–90 years. The mean rate of shoaling in this region agrees, within uncertainties, with those reported by *Feely et al*. [2012] for P16N at 0.81 ± 0.71 m yr^{-1} and P16S at 2.01 ± 0.80 m yr^{-1}. The change in saturation state at P17N translates to a decrease of −0.40 ± 0.07% yr^{-1} at 100 m, which is less than −1.24 ± 0.29% yr^{-1} reported at 100 m for the Northeast Pacific region by *Jiang et al*. [2015]. However, the P17N rate is faster than −0.27 ± 0.03 to −0.28 ± 0.04% yr^{-1} previously reported for the HOT and ALOHA, and agrees within uncertainty to 0.34 ± 0.04% yr^{-1} at P16N [*Bates et al*., 2014; *Dore et al*., 2009; *Feely et al*., 2012; *Takahashi et al*., 2014]. Comparing to the North Atlantic, where acidification rates range from 0.0017 ± 0.0001 to 0.0020 ± 0.0004 pH units yr^{-1} and decreases in aragonite saturation state from 0.26 ± 0.02 to 0.34 ± 0.07% yr^{-1}, this study suggests that P17N is among the most sensitive regions to ocean acidification in terms of high rates of pH decrease and fast shoaling of the aragonite saturation horizon.

5. Conclusions

The data from a 2012 cruise along P17N show significant changes in salinity, AOU, and DIC, relative to a 2001 CLIVAR occupation of the transect, which primarily reflect changes in circulation but also reveal deoxygenation and invasion of anthropogenic carbon dioxide in the water column of the Northeast Pacific. An extended multiple linear regression was used to estimate an increase of 7–11 μmol kg^{-1} anthropogenic CO_2 concentration in surface waters with a strong northward increase near the surface. The penetration depth of C_{anthro} decreases northward from 600 m at 33.5°N to 300 m at 50°N. As a result, C_{anthro} storage rates up to 0.55 mol m^{-2} yr^{-1} were found in the southern portion of the transect, which decrease gradually to 0.20 mol m^{-2} yr^{-1} at the northern part of the transect with an average of 0.41 ± 0.12 mol m^{-2} yr^{-1}. The increase in anthropogenic CO_2 in the Northeast Pacific resulted in a mean acidification rate of −0.002 ± 0.0009 pH units yr^{-1} and a mean shoaling of the aragonite saturation horizon of 1.8 ± 0.4 m yr^{-1}. These rates may be slightly higher than other estimates of anthropogenic carbon storage, acidification and shoaling rates in the Pacific. The Northeast Pacific is considered the end of the ocean conveyor belt. Waters found here are old, and have high DIC content and high Revelle Factors, or low buffering capacity. This causes the aragonite saturation horizon to be already quite shallow (near 125 m) compared to other regions of the ocean. As such, the Northeast Pacific is among the most sensitive regions to changes in carbonate chemistry under ocean acidification. Even though this region may not be known for its strong uptake of anthropogenic carbon, it still has the potential to store a significant amount. This study has shown that the C_{anthro} storage in the region is still increasing and that it is important to continue to monitor such changes in this region to understand its variability across time and space as well as the potential biological and ecosystem impacts of rising CO_2.

Acknowledgments
All data presented in this paper can be found at the NSF Biological and Chemical Oceanography Data Management Office (BCO-DMO) (http://www.bco-dmo.org). The authors would like to thank the Captain and crew of the R/V *New Horizon*, and to thank all the scientists, students, and volunteers who participated in the research expeditions. We would also like to express our gratitude to Amy Maas, Leocadio Blanco Bercial, Peter Wiebe, Nancy Copley, Alex Bergan, Taylor Crockford, Robert Nick Tuttle, Elliot Roberts, and Kelly Brugler for their sampling and analysis support. Thank you to Harry Hemond, Dan McCorkle, and Kevin Kroeger for their guidance. This work was funded by the National Science Foundation Ocean Acidification Program (grant OCE-1041068), National Institute of Standards and Technology (NIST-60NANB10D024), and National Science Foundation Graduate Research Fellowship Program.

References

Anderson, L. A., and J. L. Sarmiento (1994), Redfield ratios of remineralization determined by nutrient data analysis, *Global Biogeochem. Cycles*, *8*(1), 65–80, doi:10.1029/93GB03318.

Bates, N. R., Y. M. Astor, M. J. Church, K. Currie, J. E. Dore, M. Gonzalez-Davila, L. Lorenzoni, F. Muller-Karger, J. Olafsson, and J. M. Santana-Casiano (2014), A time-series view of changing surface ocean chemistry due to ocean uptake of anthropogenic CO_2 and ocean acidification, *Oceanography*, *27*(1), 126–141, doi:10.5670/oceanog.2014.16

Boyer, T. P., S. Levitus, J. I. Antonov, R. A. Locarnini, and H. E. Garcia (2005), Linear trends in salinity for the World Ocean, 1955–1998, *Geophys. Res. Lett.*, *32*, L01604, doi:10.1029/2004GL021791.

Brewer, P. G. (1978), Direct observation of the oceanic CO_2 increase, *Geophys. Res. Lett.*, *5*(12), 997–1000, doi:10.1029/GL005i012p00997.

Broecker, W. S., and T. H. Peng (1982), *Tracers in the Sea*, 690 pp., Lamont-Doherty Geol. Obs. Palisades, N. Y.

Broecker, W. S., T. Takahashi, H. J. Simpson, and T. H. Peng (1979), Fate of Fossil Fuel Carbon Dioxide and the Global Carbon Budget, *Science*, *206*(4417), 409–418, doi:10.1126/science.206.4417.409.

Brown, P. J., D. C. E. Bakker, U. Schuster, and A. J. Watson (2010), Anthropogenic carbon accumulation in the subtropical North Atlantic, *J. Geophys. Res.*, *115*, C04016, doi:10.1029/2008JC005043.
Byrne, R. H., S. Mecking, R. A. Feely, and X. Liu (2010), Direct observations of basin-wide acidification of the North Pacific Ocean, *Geophys. Res. Lett.*, *37*, L02601, doi:10.1029/2009GL040999.
Chen, C.-T. A., and F. J. Millero (1979), Gradual increase of oceanic CO_2, *Nature*, *277*, 205–206, doi:10.1038/277205a0.
Clayton, T. D., and R. H. Byrne (1993), Spectrophotometric seawater pH measurements: Total hydrogen ion concentration scale calibration of m-cresol purple and at-sea results, *Deep. Sea Res., Part I*, *40*(10), 2115–2129, doi:10.1016/0967-0637(93)90048-8.
Deutsch, C., S. Emerson, and L. Thompson (2006), Physical-biological interactions in North Pacific oxygen variability, *J. Geophys. Res.*, *111*, C09S90, doi:10.1029/2005JC003179.
Dickson, A. G., C. L. Sabine, and J. R. Christian (Eds.) (2007), Guide to Best Practices for Ocean CO_2 Measurements, PICES Special Publication 3, 191 pp.
Dickson, A. G. (2001), Reference materials for oceanic CO_2 measurements, *Oceanography*, *14*(4), 21–22.
Dickson, A. G., and F. J. Millero (1987), A comparison of the equilibrium constants for the dissociation of carbonic acid in seawater media, *Deep Sea Res. Part A*, *34*(10), 1733–1743, doi:10.1016/0198-0149(87)90021-5.
Doney, S. C., S. Yeager, G. Danabasoglu, W. G. Large, and J. C. McWilliams (2007), Mechanisms governing interannual variability of upper ocean temperature in a global hindcast simulation, *J. Phys. Oceanogr.*, *37*, 1918–1938, doi:10.1175/JPO3089.1.
Doney, S. C., I. Lima, R. A. Feely, D. M. Glover, K. Lindsay, N. Mahowald, J. K. Moore, and R. Wanninkhof (2009a), Mechanisms governing interannual variability in upper-ocean inorganic carbon system and air-sea CO_2 fluxes: Physical climate and atmospheric dust, *Deep Sea Res., Part II*, *56*(8-10), 640–655, doi:10.1016/j.dsr2.2008.12.006.
Doney, S. C., I. Lima, J. K. Moore, K. Lindsay, M. J. Behrenfeld, T. K. Westberry, N. Mahowald, D. M. Glover, and T. Takahashi (2009b), Skill metrics for confronting global upper ocean ecosystem-biogeochemistry models against field and remote sensing data, *J. Mar. Syst.*, *76*(1-2), 95–112, doi:10.1016/j.jmarsys.2008.05.015.
Dore, J. E., R. Lukas, D. W. Sadler, M. J. Church, and D. M. Karl (2009), Physical and biogeochemical modulation of ocean acidification in the central North Pacific, *Proc. Natl. Acad. Sci. U. S. A.*, *106*(30), 12,235–12,240, doi:10.1073/pnas.0906044106.
Durack, P. J., and S. E. Wijffels (2010), Fifty-Year trends in global ocean salinities and their relationship to broad-scale warming, *J. Clim.*, *23*(16), 4342–4362, doi:10.1175/2010JCLI3377.1.
Egleston, E. S., C. L. Sabine, and F. M. M. Morel (2010), Revelle revisited: Buffer factors that quantify the response of ocean chemistry to changes in DIC and alkalinity, *Global Biogeochem. Cycles*, *24*, GB1002, doi:10.1029/2008GB003407.
Falkowski, P. G., et al. (2011), Ocean deoxygenation: Past, present, and future, *Eos Trans. AGU*, *92*(46), 409–410, doi:10.1029/2011EO460001.
Feely, R. A., C. L. Sabine, T. Takahasi, and R. Wanninkhof (2001), Uptake and storage of carbon dioxide in the ocean: The global CO_2 survey, *Oceanography*, *14*(4), 18–32, doi:10.5670/oceanog.2001.03.
Feely, R. A., C. L. Sabine, R. H. Byrne, F. J. Millero, A. G. Dickson, R. Wanninkhof, A. Murata, L. A. Miller, and D. Greeley (2012), Decadal changes in the aragonite and calcite saturation state of the Pacific Ocean, *Global Biogeochem. Cycles*, *26*, GB3001, doi:10.1029/2011GB004157.
Friis, K., A. Körtzinger, J. Pätsch, and D. W. R. Wallace (2005), On the temporal increase of anthropogenic CO_2 in the subpolar North Atlantic, *Deep Sea Res., Part I*, *52*(5), 681–698, doi:10.1016/j.dsr.2004.11.017.
Gruber, N., J. L. Sarmiento, and T. F. Stocker (1996), An improved method for detecting anthropogenic CO_2 in the oceans, *Global Biogeochem. Cycles*, *10*(4), 809–837, doi:10.1029/96GB01608.
Hall, T. M., D. W. Waugh, T. W. N. N. Haine, P. E. Robbins, and S. Khatiwala (2004), Estimates of anthropogenic carbon in the Indian Ocean with allowance for mixing and time-varying air-sea CO_2 disequilibrium, *Global Biogeochem. Cycles*, *18*, GB1031, doi:10.1029/2003GB002120.
IPCC (2014), Climate Change 2014: Synthesis Report. Contribution of Working Groups I, II and III to the Fifth Assessment Report of the Intergovernmental Panel on Climate Change, edited by Core Writing Team, R. K. Pachauri and L. A. Meyer, IPCC, Geneva, Switzerland, 151 pp.
Iselin, C. O. (1939), The influence of vertical and lateral turbulence on the characteristics of the waters at mid-depths, *Eos Trans. AGU*, *20*(3), 414–417, doi:10.1029/TR020i003p00414.
Ishii, M., N. Kosugi, D. Sasano, S. Saito, T. Midorikawa, and H. Y. Inoue (2011), Ocean acidification off the south coast of Japan: A result from time series observations of CO_2 parameters from 1994 to 2008, *J. Geophys. Res.*, *116*, C06022, doi:10.1029/2010JC006831.
Jiang, L., R. A. Feely, B. R. Carter, D. J. Greeley, D. K. Gledhill, and K. M. Arzayus (2015), *Global Biogeochemical Cycles saturation state in the global oceans, Global Biogeochem. Cycles*, *29*, 1656–1673, doi:10.1002/2015GB005198.
Khatiwala, S., F. Primeau, and T. Hall (2009), Reconstruction of the history of anthropogenic CO(2) concentrations in the ocean., *Nature*, *462*(7271), 346–349, doi:10.1038/nature08526.
Khatiwala, S., et al. (2013), Global ocean storage of anthropogenic carbon, *Biogeosciences*, *10*(4), 2169–2191, doi:10.5194/bg-10-2169-2013.
Körtzinger, A., M. Rhein, and L. Mintrop (1999), Anthropogenic CO_2 and CFCs in the North Atlantic Ocean - A comparison of man-made tracers, *Geophys. Res. Lett.*, *26*(14), 2065–2068, doi:10.1029/1999GL900432.
Lamb, M. F., et al. (2002), Consistency and synthesis of Pacific Ocean CO_2 survey data, *Deep Sea Res., Part II*, *49*(1-3), 21–58, doi:10.1016/S0967-0645(01)00093-5.
Le Quéré, C., T. Takahashi, E. T. Buitenhuis, C. Rödenbeck, and S. C. Sutherland (2010), Impact of climate change and variability on the global oceanic sink of CO_2, *Global Biogeochem. Cycles*, *24*, GB4007, doi:10.1029/2009GB003599.
Levine, N. M., S. C. Doney, R. Wanninkhof, K. Lindsay, and I. Y. Fung (2008), Impact of ocean carbon system variability on the detection of temporal increases in anthropogenic CO_2, *J. Geophys. Res.*, *113*, C03019, doi:10.1029/2007JC004153.
Levitus, S., J. Antonov, and T. Boyer (2005), Warming of the world ocean, 1955-2003, *Geophys. Res. Lett.*, *32*, L02604, doi:10.1029/2004GL021592.
Liu, X., M. C. Patsavas, and R. H. Byrne (2011), Purification and characterization of meta-cresol purple for spectrophotometric seawater ph measurements, *Environ. Sci. Technol.*, *45*(11), 4862–4868, doi:10.1021/es200665d.
McPhaden, M. J., and D. Zhang (2002), Slowdown of the meridional overturning circulation in the upper Pacific Ocean, *Nature*, *415*(6872), 603–608, doi:10.1038/415603a.
Mecking, S., C. Langdon, R. A. Feely, C. L. Sabine, C. A. Deutsch, and D. H. Min (2008), Climate variability in the North Pacific thermocline diagnosed from oxygen measurements: An update based on the U.S. CLIVAR/CO_2 Repeat Hydrography cruises, *Global Biogeochem. Cycles*, *22*, GB3015, doi:10.1029/2007GB003101.
Mehrbach, C., C. H. Culberson, J. E. Hawley, and R. M. Pytkowicz (1973), Measurement of the apparent dissociation constants of carbonic acid in seawater at atmospheric pressure, *Limnol. Oceanogr.*, *18*(6), 897–907, doi:10.4319/lo.1973.18.6.0897.

Midorikawa, T., M. Ishii, S. Saito, D. Sasano, N. Kosugi, T. Motoi, H. Kamiya, A. Nakadate, K. Nemoto, and H. Y. Inoue (2010), Decreasing pH trend estimated from 25-yr time series of carbonate parameters in the western North Pacific, *Tellus, Ser. B*, *62*(5), 649–659, doi:10.1111/j.1600-0889.2010.00474.x.

Mikaloff Fletcher, S. E., et al. (2006), Inverse estimates of anthropogenic CO_2 uptake, transport, and storage by the ocean, *Global Biogeochem. Cycles*, *20*, GB2002, doi:10.1029/2005GB002530.

Murata, A., Y. Kumamoto, K. I. Sasaki, S. Watanabe, and M. Fukasawa (2009), Decadal increases of anthropogenic CO_2 along 149??E in the western North Pacific, *J. Geophys. Res.*, *114*, C04018, doi:10.1029/2008JC004920.

Pachauri, R. K., et al. (2014), *Climate Change 2014: Synthesis Report. Contribution of Working Groups I, II and III to the Fifth Assessment Report of the Intergovernmental Panel on Climate Change*.

Pardo, P. C., F. F. Pérez, S. Khatiwala, and A. F. Ríos (2014), Anthropogenic CO_2 estimates in the Southern Ocean: Storage partitioning in the different water masses, *Prog. Oceanogr.*, *120*, 230–242, doi:10.1016/j.pocean.2013.09.005.

Peng, T. H., R. Wanninkhof, and R. A. Feely (2003), Increase of anthropogenic CO_2 in the Pacific Ocean over the last two decades, *Deep Sea Res., Part II*, *50*(22-26), 3065–3082, doi:10.1016/j.dsr2.2003.09.001.

Pierrot, D., E. Lewis, and D. W. R. Wallace (2006), MS Excel program developed for CO_2 system calculations, *ORNL/CDIAC-105a*, Carbon Dioxide Inf. Anal. Cent., Oak Ridge Natl. Lab., U.S. Dep. Energy, Oak Ridge, Tenn., doi:10.3334/CDIAC/otg.CO2SYS_XLS_CDIAC105a.

Quay, P., R. Sonnerup, J. Stutsman, J. Maurer, A. Körtzinger, X. A. Padin, and C. Robinson (2007), Anthropogenic CO_2 accumulation rates in the North Atlantic Ocean from changes in the 13C/12C of dissolved inorganic carbon, *Global Biogeochem. Cycles*, *21*, GB1009, doi:10.1029/2006GB002761.

Reid, J. L. (1997), On the total geostrophic circulation of the pacific ocean: Flow patterns, tracers, and transports, *Prog. Oceanogr.*, *39*, 263–352, doi:10.1016/S0079-6611(97)00012-8.

Revelle, R., and H. E. Suess (1957), Carbon dioxide exchange between atmosphere and ocean and the question of an increase of atmospheric CO_2 during the past decades, *Tellus*, *9*(1), 18–27, doi:10.1111/j.2153-3490.1957.tb01849.x.

Roden, G. I. (1991), Subarctic-subtropical transition zone of the North Pacific: Large-scale aspects and mesoscale structure, *Biol. Oceanogr. Fish. North Pacific*, *105*, 1–38.

Sabine, C. L., and T. Tanhua (2010), Estimation of anthropogenic CO_2 inventories in the ocean, *Annu. Rev. Mar. Sci.*, *2*, 175–198, doi:10.1146/annurev-marine-120308-080947.

Sabine, C. L., R. A. Feely, R. M. Key, J. L. Bullister, F. J. Millero, K. Lee, T.-H. Peng, B. Tilbrook, T. Ono, and C. S. Wong (2002), Distribution of anthropogenic CO_2 in the Pacific Ocean, *Global Biogeochem. Cycles*, *16*(4), 1083, doi:10.1029/2001GB001639.

Sabine, C. L., et al. (2004), The oceanic sink for anthropogenic CO_2, *Science*, *305*(5682), 367–371, doi:10.1126/science.1097403.

Sabine, C. L., R. A. Feely, F. J. Millero, A. G. Dickson, C. Langdon, S. Mecking, and D. Greeley (2008), Decadal changes in Pacific carbon, *J. Geophys. Res.*, *113*, C07021, doi:10.1029/2007JC004577.

Schlitzer, R. (2015), *Ocean Data View, ODV*. [Available at odv.awi.de.]

Shulenberger, E., and J. L. Reid (1981), The Pacific shallow oxygen maximum, deep chlorophyll maximum, and primary productivity, reconsidered, *Deep Sea Res., Part A*, *28*(9), 901–919, doi:10.1016/0198-0149(81)90009-1.

Stuiver, M., P. D. Quay, and H. G. Ostlund (1983), Abyssal water carbon-14 distribution and the age of the world oceans, *Science*, *219*(4586), 849–51, doi:10.1126/science.219.4586.849.

Suzuki, T. et al. (2013), PACIFICA data synthesis project, *ORNL/CDIAC-159, NDP-092*, Carbon Dioxide Inf. Anal. Cent., Oak Ridge Natl. Lab., U.S. Dep. Energy, Oak Ridge, Tenn., doi:10.3334/CDIAC/OTG.PACIFICA_NDP092.

Takahashi, T., et al. (2009), Climatological mean and decadal change in surface ocean pCO_2, and net sea-air CO_2 flux over the global oceans, *Deep Sea Res., Part II*, *56*(8-10), 554–577, doi:10.1016/j.dsr2.2008.12.009.

Takahashi, T., S. C. Sutherland, D. W. Chipman, J. G. Goddard, and C. Ho (2014), Climatological distributions of pH, pCO_2, total CO_2, alkalinity, and $CaCO_3$ saturation in the global surface ocean, and temporal changes at selected locations, *Mar. Chem.*, *164*, 95–125, doi:10.1016/j.marchem.2014.06.004.

Talley, L. D. (1993), Distribution and formation of North Pacific Intermediate Water, *J. Phys. Oceanogr.*, *23*(3), 517–537, doi:10.1175/1520-0485(1993)023 < 0517:dafonp>2.0.co;2.

Talley, L. D., et al. (2016), Changes in ocean heat, carbon content, and ventilation: A review of the first decade of GO-SHIP global repeat hydrography, *Annu. Rev. Mar. Sci.*, *8*(1), 185–215, doi:10.1146/annurev-marine-052915-100829.

Tanhua, T., A. Körtzinger, K. Friis, D. W. Waugh, and D. W. R. Wallace (2007), An estimate of anthropogenic CO_2 inventory from decadal changes in oceanic carbon content, *Proc. Natl. Acad. Sci. U. S. A.*, *104*(9), 3037–3042, doi:10.1073/pnas.0606574104.

Tanhua, T., S. van Heuven, R. M. Key, A. Velo, A. Olsen, and C. Schirnick (2010), Quality control procedures and methods of the CARINA database, *Earth Syst. Sci. Data*, *2*(1), 35–49, doi:10.3334/CDIAC/otg.CARINA.SO.V1.0.

Wakita, M., et al. (2013), Ocean acidification from 1997 to 2011 in the subarctic western North Pacific Ocean, *Biogeosciences*, *10*(12), 7817–7827, doi:10.5194/bg-10-7817-2013.

Wallace, D. W. R. (1995), Monitoring global ocean carbon inventories, *OOSDP Background Rep.*, *5*, 54.

Wang, Z. A., and W.-J. Cai (2004), Carbon dioxide degassing and inorganic carbon export from a marsh-dominated estuary (the Duplin River): A marsh CO_2 pump, *Limnol. Oceanogr. Methods*, *49*(2), 341–354, doi:10.4319/lo.2004.49.2.0341.

Wanninkhof, R., and W. R. McGillis (1999), A cubic relationship between air-sea CO_2 exchange and wind speed, *Geophys. Res. Lett.*, *26*(13), 1889–1892, doi:10.1029/1999GL900363.

Wanninkhof, R., S. C. Doney, J. L. Bullister, N. M. Levine, M. Warner, and N. Gruber (2010), Detecting anthropogenic CO_2 changes in the interior Atlantic Ocean between 1989 and 2005, *J. Geophys. Res.*, *115*, C11028, doi:10.1029/2010JC006251.

Waters, J. F., F. J. Millero, and C. L. Sabine (2011), Changes in South Pacific anthropogenic carbon, *Global Biogeochem. Cycles*, *25*, GB4011, doi:10.1029/2010GB003988.

Waugh, D. W., T. M. Hall, B. I. McNeil, R. Key, and R. J. Matear (2006), Anthropogenic CO_2 in the oceans estimated using transit time distributions, *Tellus, Ser. B*, *58*(5), 376–389, doi:10.1111/j.1600-0889.2006.00222.x.

Whitney, F. A., H. J. Freeland, and M. Robert (2007), Persistently declining oxygen levels in the interior waters of the eastern subarctic Pacific, *Prog. Oceanogr.*, *75*(2), 179–199, doi:10.1016/j.pocean.2007.08.007.

Williams, N. L., R. A. Feely, C. L. Sabine, A. G. Dickson, J. H. Swift, L. D. Talley, and J. L. Russell (2015), Quantifying anthropogenic carbon inventory changes in the Pacific sector of the Southern Ocean, *Mar. Chem.*, *174*, 147–160, doi:10.1016/j.marchem.2015.06.015.

Wong, C. S., J. R. Christian, S. K. Emmy Wong, J. Page, L. Xie, and S. Johannessen (2010), Carbon dioxide in surface seawater of the eastern North Pacific Ocean (Line P), 1973-2005, *Deep Sea Res., Part I*, *57*(5), 687–695, doi:10.1016/j.dsr.2010.02.003.

Yao, W., X. Liu, and R. H. Byrne (2007), Impurities in indicators used for spectrophotometric seawater pH measurements: Assessment and remedies, *Mar. Chem.*, *107*(2), 167–172, doi:10.1016/j.marchem.2007.06.012.